American Mineralogist, Volume 76, pages 928–941, 1991

Al,Si exchange kinetics in sanidine and anorthoclase and modeling of rock cooling paths

HERBERT KROLL, REGINA KNITTER*
Institut für Mineralogie, Westfälische Wilhelms-Universität, Corrensstr. 24, D-4400 Münster, Germany

ABSTRACT

The kinetics of the Al,Si exchange in alkali feldspars has been investigated for the two topochemically monoclinic samples sanidine (Or84) and anorthoclase (Or28). The crystals were first disordered at 1050 °C and then reordered at 850 °C, $P(H_2O) = 0.5$ kbar; at 750 °C, 1 kbar; and at 650 °C, 1 kbar. Disordering experiments were performed with natural, untreated sanidine at the same conditions to bracket the equilibrium ordering state. The Al,Si distribution was determined from the optic axial angle $2V_X$, as measured on a spindle stage. The kinetic data were evaluated with the Mueller-Ganguly formalism. It was found that the ordering kinetics in sanidine and anorthoclase are similar. Steady states were reached after ≈10 d at 850 °C, after ≈100 d at 750 °C, and would be reached after several years at 650 °C. Activation energies are 223.0 (± 11.3) kJ/mol for sanidine and 244.3 (± 56.1) kJ/mol for anorthoclase. Their respective apparent equilibrium temperatures T_{ae} are 685(38) °C and 798(33) °C, and probably represent temperatures prior to the volcanic eruption. Model calculations of cooling paths show that, if cooling starts at $T_0 > (T_{ae} + 50$ °C), then the cooling rate at $T \approx (T_{ae} + 50$ °C) can be recovered from the final ordering state achieved. The actual temperature T_0 at which cooling begins and the cooling rate between T_0 and $T_{ae} + 50$ °C do not influence the final state of order. However, if continuous cooling begins at a temperature T_0 in the interval between $T_{ae} + 50$ °C and T_{ae}, T_0 must be known to determine the cooling rate.

INTRODUCTION

The kinetics and mechanisms of ordering and disordering reactions in alkali feldspars have been the subject of many papers (e.g., MacKenzie, 1957; Eberhard, 1967; Martin, 1969; Müller, 1970; Senderov and Yas'kin, 1975, 1976; Mason, 1979; Yund and Tullis, 1980; Blasi et al., 1984; Goldsmith and Jenkins, 1985; Goldsmith, 1988). However, apart from albite (McConnell and McKie, 1960; McKie and McConnell, 1963), no attempt has been made to extract kinetic data that are suitable for reconstructing cooling paths of rocks. In order to calculate the increase in Al,Si order during a continuous cooling process, it is necessary to know the temperature dependences of the equilibrium constants and rate constants. These data will be presented in this paper for topochemically monoclinic sanidine (Or84) and anorthoclase (Or28).

Calculations of cooling paths were first presented by Seifert and Virgo (1975) and Seifert (1977), based on kinetic data obtained from orthoamphiboles. Since then, several papers have appeared that consider the Fe^{2+},Mg exchange kinetics in Fe^{2+},Mg silicates, notably pyroxene and amphibole (e.g., Besancon, 1981; Skøgby, 1987; Saxena et al., 1987; Anovitz et al., 1988). Very helpful reviews of the method for extracting kinetic data from isothermal experiments have been given by Ganguly (1982) and Ganguly and Saxena (1987).

THEORY

In monoclinic alkali feldspars, $(K,Na)AlSi_3O_8$, there are two eightfold tetrahedral sites, T_1 and T_2, onto which Al and Si are distributed according to the exchange reaction

$$\underset{\text{order}}{Al(T_1)} + Si(T_2) \rightleftharpoons \underset{\text{antiorder}}{Al(T_2)} + Si(T_1). \quad (1)$$

The atomic fraction of Al in T_1 is $X^{T1}_{Al} = 0.5$ in an ordered monoclinic alkali feldspar, $X^{T1}_{Al} = 0.25$ in a disordered crystal, and $X^{T1}_{Al} = 0$ in a hypothetically antiordered crystal. Actual values for sanidine lie in the range $\approx 0.35 > X^{T1}_{Al} > \approx 0.27$. as a result of stoichiometry and site occupancy constraints, all atomic fractions in Equation 1 can be given in terms of X^{T1}_{Al}:

$$X^{T2}_{Al} = 0.5 - X^{T1}_{Al}, \qquad X^{T1}_{Si} = 1 - X^{T1}_{Al},$$
$$X^{T2}_{Si} = 0.5 + X^{T1}_{Al}. \quad (2)$$

In the Mueller-Ganguly formalism (Mueller, 1967, 1969; Ganguly, 1982; Ganguly and Saxena, 1987), the basic rate equation for the ideal Al,Si exchange process (Eq. 1) is written as a balanced reaction:

$$-\frac{dX^{T1}_{Al}}{dt} = 0.5 \cdot C_o(\vec{k} X^{T1}_{Al} X^{T2}_{Si} - \overleftarrow{k} X^{T2}_{Al} X^{T1}_{Si}). \quad (3)$$

Equation 3 implies that in an isothermal experiment

* Present address: Kernforschungszentrum Karlsruhe, Institut für Material- und Festkörperforschung III, Postfach 3640, D-7500 Karlsruhe, Germany.

0003–004X/91/0506–0928$02.00

the decrease with time t of Al in T_1 is taken to be proportional to the joint probability of finding Al in T_1 and Si in T_2. Likewise, the increase with time of Al in T_1 is proportional to the joint probability of finding Al in T_2 and Si in T_1. The terms $\vec{k}$ and $\overleftarrow{k}$ are the rate constants for the forward (disordering) and reverse (ordering) reactions; C_o is the total number of $T_1 + T_2$ sites per unit volume. At equilibrium, the disordering and ordering rates are equally effective, so that

$$-\frac{dX_{Al}^{T_1}}{dt} = 0$$

$$\frac{C_o\vec{k}}{C_o\overleftarrow{k}} = \frac{X_{Al}^{T_2}\cdot X_{Si}^{T_1}}{X_{Al}^{T_1}\cdot X_{Si}^{T_2}} = K_d. \quad (4)$$

On the basis of Equations 2 and 4, the rate equation (Eq. 3) can be rewritten as

$$-\frac{dX_{Al}^{T_1}}{dt} = C_o\vec{k}[a(X_{Al}^{T_1})^2 + bX_{Al}^{T_1} + c] \quad (5)$$

where $a = 0.5(1 - K_d^{-1})$, $b = 0.25 + 0.75K_d^{-1}$, and $c = -0.25K_d^{-1}$. Since $(b^2 - 4ac) > 0$, integration of Equation 5 results in

$$-C_o\vec{k}\cdot\Delta t = d^{-1}\left(\ln\frac{|2aX_{Al}^{T_1} + b - d|}{2aX_{Al}^{T_1} + b + d}\right)_{X_{Al}^{T_1}(t_o)}^{X_{Al}^{T_1}(t)} \quad (6)$$

where $d = (b^2 - 4ac)^{1/2}$, and $\Delta t = t - t_o$ is the duration of the experiment. Solving for $X_{Al}^{T_1}(t)$ gives

$$X_{Al}^{T_1}(t) = -\frac{b}{2a} + \frac{d}{2a}\cdot\frac{1 + ef}{1 - ef} \quad (7)$$

where

$$e = \frac{2aX_{Al}^{T_1}(t_o) + b - d}{2aX_{Al}^{T_1}(t_o) + b + d}$$

$$f = \exp(-C_o\vec{k}\cdot\Delta t\cdot e).$$

Equation 7 is suitable for calculating the isothermal change of Al in T_1. In the case of continuous cooling, the ordering process can be approximated by substituting small steps of quenching and isothermal annealing for the continuous cooling process, as suggested by Ganguly (1982). A prerequisite for these calculations is the determination of the temperature dependences of K_d and $C_o\vec{k}$, which will be presented in this paper.

It is well known that the rate of ordering not only depends on temperature, but also on the availability of H_2O and on the H_2O vapor pressure. These factors will be investigated in a forthcoming paper.

Experimental methods

Starting material

Two samples of topochemically monoclinic alkali feldspars have been studied. These are sanidine from Volkesfeld, Eifel, Germany, and anorthoclase from Puerto Rico, Gran Canaria, Canary Islands. The Volkesfeld sanidine occurs embedded in tuff as large, smoky crystals that sometimes have gemlike quality. Two large single crystals, denoted VS1 and VS2, were selected for investigation. The anorthoclase is found in an ignimbrite as clear crystals with a grain size of 0.3–0.5 mm. The major element composition was determined by electron probe microanalysis (Table 1).

Table 1. Chemical composition

	An $CaAl_2Si_2O_8$	Ab $NaAlSi_3O_8$ (mol%)	Or $KAlSi_3O_8$
Sanidine VS1	0.1(1)	15.8(5)	84.1(5)
Sanidine VS2	0.1(1)	15.6(9)	84.4(9)
Anorthoclase 1363	0.8(3)	71.7(8)	27.5(9)

The two Volkesfeld crystals were crushed and sieved to a size of ≈0.5 mm. Sample VS2 was heated dry at 1050 °C for 18 d to disorder it. The anorthoclase crystals were also heated dry at 1050 °C, 6 d, to disorder them and to remove incipient exsolution.

Subsequently, the unheated VS1 sanidine, the heated VS2 sanidine, and the heated anorthoclase were sealed in Au capsules and hydrothermally annealed in Bridgman-type autoclaves at 650 °C and 750 °C, 1 kbar; and 850 °C, 0.5 kbar. Experiment durations varied from 0.25 d to 128 d. In order to test the effect of H_2O content and alkali excess on the Al,Si exchange kinetics, the amount of H_2O in the capsules was varied and a series of experiments was performed at 650 °C with 20 wt% $(K_{0.85}Na_{0.15})_2[Si_2O_5]$ added to the samples. The composition of the sanidine crystals, which were annealed with disilicate, was checked later and found not to have changed. The annealing conditions are listed in Table 2.

Temperatures at 650 °C and 750 °C were monitored using Ni/Cr-Ni thermocouples, those at 850 °C were monitored using Pt/Rh-Pt thermocouples. Accuracy is estimated to be ±10 °C. For the short experiments at 850 °C (0.25 d, 0.5 d, 1 d), the furnace was preheated at 900 °C and regulated to 850 °C when the autoclave had reached 780 °C. In this way, the period of heating from room temperature to 850 °C was minimized, such that the sam-

Table 2. Annealing conditions for sanidine and anorthoclase

Sample	H_2O content (wt%)	650 °C, 1 kbar	750 °C, 1 kbar	850 °C, 0.5 kbar
		Sample weight (mg)		
VS1	10	170	170	170
VS2(h)*	10	240	240	240
VS2(h)	wet**	100	100	
VS2(h)	dry†			100
VS2(h) + DS‡	10	170		
1363(h)	10	100	100	100

* The designation (h) indicates that the sample had previously been annealed at 1050 °C.

** The fluid phase in the autoclave was given access to the samples by boring a small hole into the Au capsules.

† The samples were sealed in the Au capsules without adding H_2O.

‡ The amount of 20 wt% $(K_{0.85}Na_{0.15})_2Si_2O_5$ was added to the samples.

TABLE 3. Lattice parameters of sanidine

Sample	Annealing conditions T (°C)	t (d)	a (Å)	b (Å)	c (Å)	β (°)	$2V_x$ (°)	$2X_{Al}^{T_1}$*
VS2(h)**	1050	18	8.5442(8)	13.0316(10)	7.1745(7)	115.980(5)	40.80	0.543(4)
VS2(h)	750	4	8.5433(5)	13.0286(5)	7.1765(4)	115.981(3)	36.38	0.559(2)
VS2(h)	750	16	8.5439(8)	13.0258(9)	7.1779(7)	115.984(5)	29.95	0.575(4)
VS1	750	32	8.5432(9)	13.0224(9)	7.1799(7)	115.999(5)	24.35	0.594(4)
VS1	750	4	8.5436(6)	13.0215(6)	7.1817(5)	115.995(4)	18.40	0.604(3)
VS1			8.5423(5)	13.0205(6)	7.1820(4)	115.997(3)	13.70	0.610(3)

Note: Estimated standard errors in parentheses refer to last digits.

* The values of $2X_{Al}^{T_1}$ were calculated from Equation 8. The errors given are calculated from the standard errors in the b and c cell parameters using the error propagation law.

** The designation (h) indicates that the original sample had been annealed at 1050 °C, 18 d, prior to further heat treatment.

ples remained less than 10 min in the temperature interval between 670 °C and 850 °C. After the experiments, the autoclaves were quenched in H_2O and cooled to room temperature within 5 min.

Measurement of $2V_x$

The optic axial angle $2V_x$ of alkali feldspars is a sensitive measure of Al,Si distribution (Su et al., 1984, 1986). We monitored changes in this parameter during the isothermal experiments by measuring $2V_x$ conoscopically on a spindle stage (Medenbach, 1985). The optic axial plane is oriented $\parallel(010)$ in the sanidine crystals and $\approx\perp(010)$ in the anorthoclase crystals. The optic normal was adjusted parallel to the spindle axis. Five crystals were selected from each experiment. For each crystal, $2V_x$ was measured twice at 589 nm. Reproducibility was better than $\pm 0.2°$. To match n_Y of the sanidine and anorthoclase crystals, we chose n_D of the immersion liquid as 1.524 and 1.528, respectively. In our experiments, n_Y varied to a negligible degree.

Conversion of $2V_x$ into tetrahedral Al content $X_{Al}^{T_1}$

Kroll and Ribbe (1983) investigated the influence of the Al,Si distribution in alkali feldspars on the b and c cell parameters. To calculate the Al content of the T_1 tetrahedral site in topochemically monoclinic specimens, they gave the following equation:

$$2X_{Al}^{T_1} = -7.590 - 2.3258b + 5.3581c. \quad (8)$$

In a subsequent paper, Kroll and Ribbe (1987) suggested the use of the b and c^* cell parameters, rather than b and c, to calculate Al content because plots of b vs. c^* show an improved linearity. This paper is based on the data given in Knitter (1985), in which Equation 8 of Kroll and Ribbe (1983) was used. However, the new equations

TABLE 4. Lattice parameters of anorthoclase

Sample	Annealing conditions T (°C)	t (d)	a (Å)	b (Å)	c (Å)	α, β, γ (°)	$2V_x$ (°)	$2X_{Al}^{T_1}$*
1363	1050	6	8.2819(8)	12.9634(7)	7.1500(5)	91.568(6) 116.302(4) 90.138(4)	39.00	0.570(3)
1363(h)**	750	1	8.2801(8)	12.9627(7)	7.1508(5)	91.529(6) 116.292(5) 90.139(5)	41.00	0.576(3)
1363(h)	850	4	8.2789(8)	12.9633(7)	7.1508(5)	91.546(6) 116.291(4) 90.132(5)	42.22	0.575(3)
1363(h)	850	8	8.2811(10)	12.9598(8)	7.1515(7)	91.522(7) 116.300(6) 90.125(6)	44.25	0.587(4)
1363(h)	750	16	8.2796(7)	12.9615(6)	7.1512(5)	91.521(6) 116.299(4) 90.103(4)	44.47	0.581(3)
1363(h)	750	32	8.2792(9)	12.9611(8)	7.1533(7)	91.521(7) 116.293(5) 90.127(5)	47.07	0.593(4)

Note: Estimated standard errors in parentheses refer to last digits.

* The values of $2X_{Al}^{T_1}$ are calculated from Equation 8. The errors given are calculated from the standard errors in the b and c cell parameters using the error propagation law.

** The designation (h) indicates that the original sample had been annealed at 1050 °C, 6 d, prior to further heat treatment.

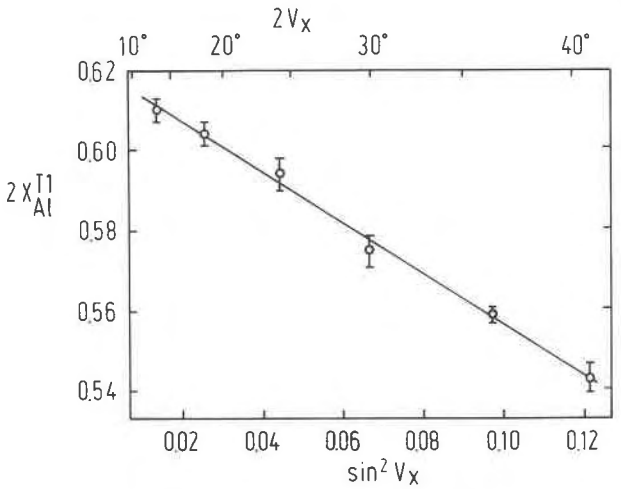

Fig. 1. Al content $2X^{T_1}_{Al}$ in the T_1 tetrahedral sites of sanidine vs. $\sin^2 V_X$. The values of $2X^{T_1}_{Al}$ are calculated from Equation 8. The error in $2X^{T_1}_{Al}$ results from the standard deviations in the b and c cell parameters (Table 3). The error in $\sin^2 V_X$ is less than symbol size, assuming the error in $2V_X$ of a single crystal to be $\pm 0.2°$.

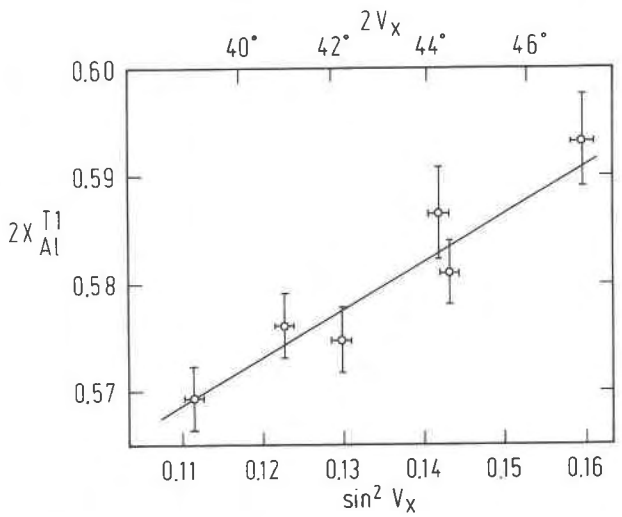

Fig. 2. Al content $2X^{T_1}_{Al}$ in the T_1 tetrahedral sites of anorthoclase vs. $\sin^2 V_X$. The values of $2X^{T_1}_{Al}$ are calculated from Equation 8. The error in $2X^{T_1}_{Al}$ results from the standard deviations in the b and c cell parameters (Table 4). The error in $\sin^2 V_X$ is calculated assuming $2V_X$ of a single crystal is in error by $\pm 0.2°$.

give results that are very similar to the old ones for Na- and K-rich compositions. We therefore considered it unnecessary to recalculate site occupancies.

Six single crystals of sanidine and anorthoclase, which cover the range of $2V_X$ values observed in this study, were selected to calibrate $2V_X$ vs. $X^{T_1}_{Al}$. After measuring $2V_X$, the crystals were powdered and their lattice parameters determined using the Guinier-Jagodzinski technique (Kroll et al., 1980). To obtain consistent results, the same 64 and 55 powder lines were indexed in each pattern of sanidine and anorthoclase, respectively, and used for the refinement. Tables 3 and 4 show that the variation of b and c is small: 0.011 Å and 0.008 Å, respectively, for sanidine, and only 0.004 Å and 0.003 Å, respectively, for anorthoclase. Nevertheless, on the basis of careful measurement and selection of diffraction lines, these small variations are clearly resolved.

In Figures 1 and 2, $\sin^2 V_X$ is plotted vs. $X^{T_1}_{Al}$ obtained from Equation 8. Linear regression yields the following results:

$$2X^{T_1}_{Al} = 0.6197(13) - 0.6308(183)\cdot\sin^2 V_X \quad (R^2 = 0.997) \tag{9a}$$

for sanidine, and

$$2X^{T_1}_{Al} = 0.5197(104) + 0.4458(764)\cdot\sin^2 V_X \quad (R^2 = 0.885) \tag{9b}$$

for anorthoclase.

Within a given temperature range, the variation of the optic axial angle is much smaller in anorthoclase than it is in sanidine, namely $\Delta 2V_X = 6°$ compared to 28°. For this reason, and because of the larger variability of chemical composition, the correlation between $\sin^2 V_X$ and $X^{T_1}_{Al}$ is not as good in anorthoclase as in sanidine.

Experimental results for sanidine

Variation of $2V_X$

From each hydrothermal experiment, five single crystals were selected for the measurement of $2V_X$. The average values are listed in Table 5. The variation of $2V_X$ within each group of measurements is small for the VS1 sample with an overall standard deviation of $\pm 0.35°$, but considerably larger for the preheated VS2(h) sample, where the overall standard deviation is 1.5°. Occasionally, $2V_X$ varies from one edge to the other in a given crystal. It must be emphasized, however, that zoning in terms of rim and core has not been observed. In most cases, the crystals are homogeneous with respect to the distribution of $2V_X$.

The range of $2V_X$ measured within each group of five VS2(h) crystals decreases when equilibrium states of order are approached. An analogous phenomenon is reported by Güttler et al. (1989), who monitored the disordering of low albite by measuring the positional change of the 131 and $1\bar{3}1$ lines in a powder pattern.

As is seen from Table 5, the results of the experiments performed on the VS2(h) sample under various conditions do not show any significant differences. We ascribe the variations of $\langle 2V_X \rangle$ to the random sampling of five single crystals from each experiment. In particular, (1) the Al,Si exchange rate was not increased when more than 10 wt% H_2O was present in the Au capsules, as is seen from a comparison of the VS2(h)—wet—results with the VS2(h) results. (2) When the crystals that had been sealed in the Au capsules without H_2O (dry experiments at 850 °C) were recovered from the capsules, they appeared to be slightly humid, although in no case could any leakage be detected. The dry experiments, therefore,

TABLE 5. Correlation of the optic axial angle with the degree of order of sanidine (Eq. 9a)

T	650 °C VS1		650 °C VS2(h)					750 °C VS1	
t (d)	$\langle 2V_x \rangle$	$X_{Al}^{T_1}$	$\langle 2V_x \rangle^A$	$\langle 2V_x \rangle^B$	$\langle 2V_x \rangle^C$	$\langle\langle 2V_x \rangle\rangle$	$X_{Al}^{T_1}$	$\langle 2V_x \rangle$	$X_{Al}^{T_1}$
0.25									
0.5									
1								16.05	0.3037(3)
2	15.06	0.3044(3)	39.87	39.68	40.53	40.03	0.2729(18)	17.47	0.3026(3)
4	15.35	0.3042(3)	39.34	38.94	40.74	39.67	0.2735(18)	18.94	0.3013(3)
8	14.22	0.3053(2)	39.79	40.30	39.01	39.70	0.2735(18)	20.85	0.2995(3)
16	13.53	0.3055(2)	37.30	38.69	37.81	37.93	0.2765(17)	23.62	0.2967(4)
32	10.08	0.3074(2)	37.15	38.04	37.57	37.59	0.2771(17)	24.41	0.2958(4)
64	8.15	0.3083(1)	34.95	33.21	32.86	33.67	0.2834(15)	24.03	0.2962(4)
128	3.35	0.3096(1)	28.60	28.11	29.88	28.86	0.2903(13)		

Initial samples	$\langle 2V_x \rangle$	$X_{Al}^{T_1}$
Untreated VS1	14.30	0.3050(2)
VS2 after heating	40.01	0.2730(18)

Note: The $\langle 2V_x \rangle$ is the average $2V_x$ value measured on five single crystals selected from each experiment; $\langle\langle 2V_x \rangle\rangle$ is the grand mean $2V_x$ value from which $X_{Al}^{T_1}$ is calculated. A = VS2(h), B = VS2(h)—wet, C = VS2(h) + DS, D = VS2(h)—dry (compare Table 2).

were not truly dry, but were performed with a small, unknown content of H_2O. As a result, the rate of change of $\langle 2V_X \rangle$ is the same as in the VS2(h) experiments. This is not surprising because it is known from the work of Yund (1986), Goldsmith (1988), and Snow and Yund (1988) that only a very small amount of H_2O is required to enhance the Al,Si exchange kinetics compared to truly anhydrous experiments. (3) In contrast to Martin's (1969) experiments, the addition of potassium sodium disilicate did not affect the exchange kinetics. This is in agreement with Mason (1979) who states that above a certain temperature (≈700 °C) the ordering kinetics is not influenced by any admixture.

It should be noted that most previous experiments were performed on alkali feldspars crystallized from gels or glasses. The crystals so produced are imperfect and very small. Their ordering kinetics may be affected by solution-redeposition processes (Mason, 1980), whereas such a disturbing influence can be excluded with the large crystals used in our experiments.

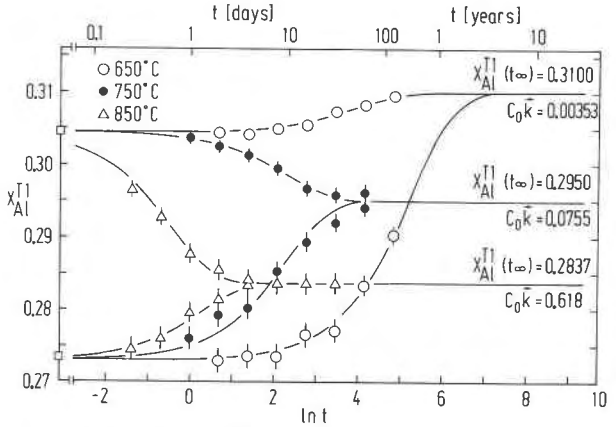

Fig. 3. Ordering and disordering with time in sanidine. Rate constants $C_o\vec{k}$ of the ordering process and equilibrium values $X_{Al}^{T_1}$ (t_∞) are given for each temperature.

The mean values of $2V_X$ in Table 5 were converted into site occupancies $X_{Al}^{T_1}$ using Equation 9a. For the VS1 samples, we have assumed a standard error of ±0.35° in $\langle 2V_X \rangle$ throughout, from which the error in $X_{Al}^{T_1}$ was calculated using the error propagation law. The standard error of $\langle 2V_X \rangle$ for the VS2(h) samples was given above as ±1.5°. We have assumed an error of ±1° for the overall mean $2V_X$ values calculated from the groups of two and three $\langle 2V_X \rangle$ data.

The values of $X_{Al}^{T_1}$ so obtained are plotted vs. time in Figure 3. At 850 °C and 750 °C, equilibrium states of order are approached by both natural and preheated samples within ≈10 and ≈100 d, respectively. At 650 °C, even the natural sample still orders somewhat. It would approach equilibrium after several years. Although the increase in order only affects the third decimal place of $X_{Al}^{T_1}$, it is clearly resolved as a result of the sensitive reaction of $2V_X$.

The curves in Figure 3 were drawn using Equation 7, with the rate constant $C_o\vec{k}$ chosen so that an optimal fit of the data was obtained. Rate constants so derived are listed in Table 6 together with equilibrium constants and equilibrium Al,Si distributions for the 750 °C and 850 °C experiments. Steady state values of the 650 °C and 1050 °C experiments are assumed to represent equilibrium.

It is known from the work of Zeipert and Wondratschek (1981) and Bertelmann et al. (1985) that untreated sanidine from Volkesfeld shows an unusually rapid change of order when heated dry, which justifies our assumption that equilibrium was reached at 1050 °C. The reason for the rapid Al,Si exchange is not yet clear. During the heating experiment, the exchange rate slows, and the kinetics finally become normal. In this sense, we consider the VS2(h) sample to represent the normal kinetic behavior of sanidine. We heated the untreated sanidine sample together with the preheated one to demonstrate equilibrium, as opposed to steady states, at 850 °C and 750 °C and to better constrain equilibrium at 650 °C. In the following treatment, we will refer to rate constants obtained

TABLE 5—*Continued*

750 °C VS2(h)				850 °C VS1		850 °C VS2(h)			
$\langle 2V_x\rangle^A$	$\langle 2V_x\rangle^B$	$\langle\langle 2V_x\rangle\rangle$	$X_{Al}^{T_1}$	$\langle 2V_x\rangle$	$X_{Al}^{T_1}$	$\langle 2V_x\rangle^A$	$\langle 2V_x\rangle^D$	$\langle\langle 2V_x\rangle\rangle$	$X_{Al}^{T_1}$
				23.88	0.2964(4)	39.08	39.31	39.20	0.2744(17)
				26.96	0.2927(4)	38.58	38.02	38.30	0.2759(17)
37.60	38.73	38.17	0.2761(17)	30.84	0.2876(5)	35.81	36.50	36.16	0.2795(16)
36.51	36.14	36.33	0.2792(16)	32.27	0.2855(5)	34.90	35.08	34.99	0.2813(16)
35.29	36.10	35.70	0.2802(16)	33.24	0.2841(5)	33.50	33.95	33.73	0.2833(15)
33.04	31.80	32.42	0.2853(15)	33.43	0.2838(5)	33.43	33.71	33.57	0.2835(15)
29.72	29.26	29.49	0.2894(14)	33.58	0.2835(5)	33.63	33.49	33.56	0.2836(15)
27.23	27.88	27.56	0.2920(13)	33.48	0.2837(5)	33.48	33.49	33.49	0.2837(15)
26.48	25.31	25.90	0.2940(12)						

from the VS2(h) sample only. It may be noted, however, that the Al,Si exchange kinetics of the untreated sanidine are not as fast under hydrothermal conditions as one might expect from the dry experiments of Bertelmann et al. (1985). In fact, at 750 °C the rate constants for the untreated and the preheated material are virtually the same (see Table 6).

Rate constants and equilibrium constants

Rate constants listed in Table 6 are plotted in Figure 4. Regression analysis results in the following Arrhenius equation:

$$\ln C_o\vec{k} = 23.51\ (\pm\ 1.34) - 26854\ (\pm\ 1359)/T \qquad (R^2 = 0.997) \qquad (10)$$

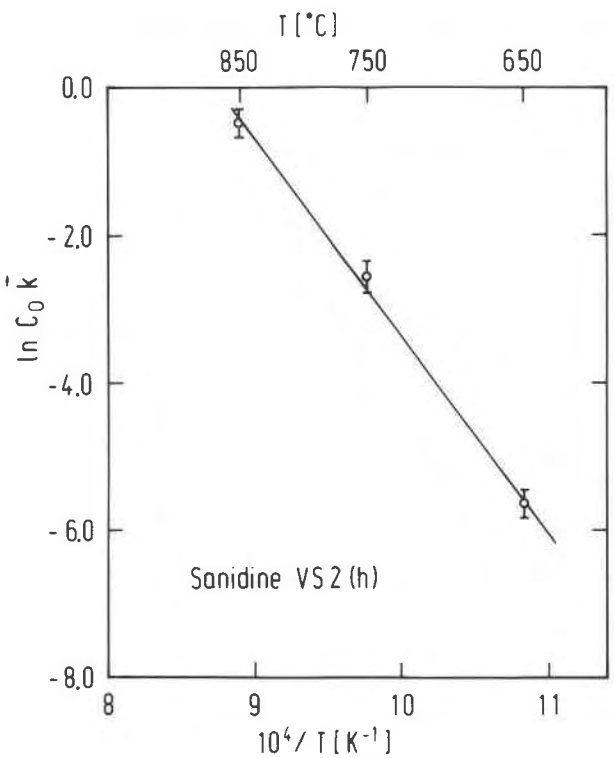

Fig. 4. Arrhenius diagram for rate constants $C_o\vec{k}$ in sanidine. The values of $C_o\vec{k}$ were taken from Figure 3.

which yields the activation energy of the disordering process $\vec{E}_A = 223.0\ (\pm\ 11.3)$ kJ/mol.

It should be emphasized that the experiments at 650 °C and 750 °C have been performed at $P(H_2O) = 1$ kbar, whereas $P(H_2O)$ was 0.5 kbar at 850 °C. This means that the data in the Arrhenius plot are not, strictly speaking, comparable. However, further experiments in which $P(H_2O)$ was systematically varied showed that at 850 °C the rate constants are almost unaffected by an increase of $P(H_2O)$ to 1 kbar (Papageorgiou, personal communication). We assume therefore that the calculated activation energy is representative for $P(H_2O) = 1$ kbar.

The pressure difference of 0.5 kbar is not expected to affect the Al,Si equilibrium distribution to a measurable degree because the molar volume of sanidine is virtually unaffected by the Al,Si distribution.

The equilibrium constants plotted in Figure 5 follow a curvilinear fit. This is a consequence of the nonconvergent character of the disordering process. The T_1 and T_2 sites are nonequivalent by symmetry and the energetic difference between them causes unequal partitioning of Al. The slope of the curve in Figure 5 is therefore expected to become more gentle as disorder is approached.

Orthopyroxene also shows nonconvergent disordering with regard to the distribution of Fe^{2+} and Mg on the M2 and M1 sites, with Fe^{2+} strongly preferring the M2 site. The temperature dependence of the Fe,Mg distribution calculated from equations given by Ganguly (1982) and Anovitz et al. (1988) is qualitatively the same as the temperature dependence of the Al,Si distribution in sanidine.

TABLE 6. Rate constants $C_o\vec{k}$, equilibrium constants K_d, and Al,Si equilibrium distributions $X_{Al}^{T_1}(t_\infty)$ for sanidine

			VS1	VS2(h)
T (°C)	$X_{Al}^{T_1}(t_\infty)$	K_d	$C_o\vec{k}$ (d^{-1})	$C_o\vec{k}$ (d^{-1})
650	0.3100(15)	0.5221(88)	0.01300(260)	0.00353(71)
750	0.2950(10)	0.6162(67)	0.0755 (151)	0.0755 (151)
850	0.2837(05)	0.6969(38)	1.300 (260)	0.618 (124)
1050	0.2730(10)	0.7820(84)		

Note: Errors given in parentheses refer to the last digits. The errors in $X_{Al}^{T_1}$ were estimated from the fit of data in Figure 3, those of K_d were calculated from the error propagation law applied to Equation 4. The error in $C_o\vec{k}$ was assumed to be ±20%.

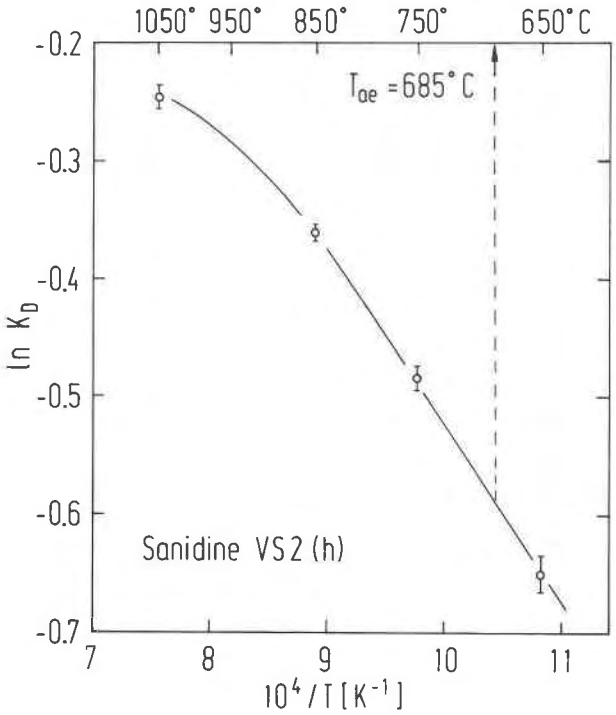

Fig. 5. Equilibrium distribution coefficients K_d of sanidine vs. temperature. The values of K_d were calculated from X_{Al}^{T1} (t_∞) given in Figure 3.

Salje and Kroll (1991) have developed a Landau potential to describe nonconvergent disordering. They show that, in the most simple approximation, the inverse of the macroscopic order parameter, Q, where $Q = 4X_{Al}^{T1} - 1$, should vary linearly with temperature, whereas ln K_d should vary nonlinearly with $1/T$.

At lower temperatures, the ln K_d curve in Figure 5 roughly approximates a straight line. A fit through the three low temperature data points gives

$$\ln K_d = 0.977\ (\pm\ 0.042) - 1500\ (\pm\ 43)/T \quad (R^2 = 0.999). \qquad (11a)$$

Following an alternative suggestion by O'Neill and Navrotsky (1983, 1984), $-RT \ln K_d$ was plotted vs. X_{Al}^{T2} ($= 0.5 - X_{Al}^{T1}$) resulting in a linear relation over the whole temperature range:

$$-RT \ln K_d = 16.79\ (\pm\ 0.25) - 61.98\ (\pm\ 1.20) \cdot X_{Al}^{T2}\ \text{(kJ/mol)}. \qquad (11b)$$

The intercept of the straight line can be interpreted as an Al,Si interchange enthalpy. The value of 16.8 kJ/mol compares favorably with the enthalpy difference between the antiordered and ordered states as found by Hovis (1988, Eq. 6): 18.4 kJ/mol.

From Equation 11a, we obtain the apparent equilibrium temperature T_{ae} of the natural sanidine with $X_{Al}^{T1} = 0.3045(2)$ as $T_{ae} = 685(38)$ °C. It may be noted that the error in T_{ae} is mainly caused by the error in the slope and intercept of Equation 11a, whereas the error in X_{Al}^{T1} contributes very little to the uncertainty in T_{ae}.

Experimental results for anorthoclase

Variation of $2V_X$

To determine $\langle 2V_X \rangle$ in anorthoclase we followed the same procedure as with sanidine. However, in anorthoclase the range of $\langle 2V_X \rangle$ observed is much smaller (compare Tables 7 and 5). As in sanidine, we assumed an error of ±1° to be associated with $\langle 2V_X \rangle$, from which the error in X_{Al}^{T1} given in Table 7 was calculated.

Rate constants and equilibrium constants

The variation with time of X_{Al}^{T1} is plotted in Figure 6. Steady states assumed to represent equilibrium are reached after experiment durations similar to those with sanidine. Rate constants, equilibrium constants, and Al,Si equilibrium distributions are listed in Table 8. The activation energy for the disordering process is obtained from the Arrhenius plot in Figure 7:

$$\ln C_o\vec{k} = 25.40\ (\pm\ 6.66) - 29402\ (\pm\ 6747)/T \quad (R^2 = 0.950)$$
$$\vec{E}_A = 244.3\ (\pm\ 56.1)\ \text{kJ/mol}. \qquad (12)$$

Table 7. Correlation of the optic axial angle with the degree of order of anorthoclase (Eq. 9b)

t	T = 650 °C		750 °C		850 °C	
(d)	$\langle 2V_X \rangle$	X_{Al}^{T1}	$\langle 2V_X \rangle$	X_{Al}^{T1}	$\langle 2V_X \rangle$	X_{Al}^{T1}
0.25					40.75	0.2869(13)
0.5					39.79	0.2857(12)
1			41.00	0.2872(13)	40.41	0.2864(12)
2	39.61	0.2854(12)	41.31	0.2876(13)	41.20	0.2874(13)
4	39.27	0.2850(12)	42.15	0.2887(13)	42.22	0.2888(13)
8	39.43	0.2852(12)	44.81	0.2922(14)	44.25	0.2915(13)
16	39.75	0.2856(12)	44.47	0.2918(13)	44.17	0.2914(13)
32	39.65	0.2855(12)	47.07	0.2954(14)	44.35	0.2916(13)
64	39.85	0.2857(12)	47.28	0.2957(14)		
128	40.54	0.2866(13)				

Initial samples	$\langle 2V_X \rangle$	X_{Al}^{T1}
Untreated	45.83	0.2936(14)
Heated at 1050 °C	39.00	0.2847(12)

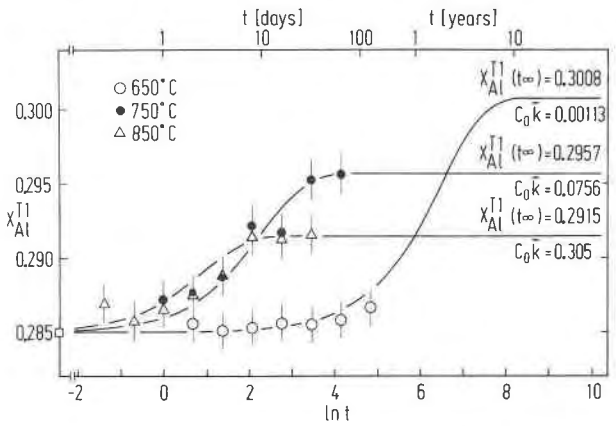

Fig. 6. Ordering with time in anorthoclase. Rate constants $C_o\vec{k}$ and equilibrium values $X_{Al}^{T_1}$ (t_∞) are given for each temperature.

With anorthoclase, we do not have further information on the pressure dependence of the rate constant at 850 °C. Apart from the larger error, $\vec{E}_A$ is therefore not as reliable as with sanidine.

The values of ln K_d approximate a straight line (Fig. 8). In calculating the regression equation

$$\ln K_d = 0.0222(11) - 525.8(1.3)/T \qquad (R^2 = 0.999) \qquad (13)$$

the data point at 650 °C has been omitted, because equilibrium is poorly defined at this temperature (Fig. 6).

Unlike sanidine, the approximate straight line behavior includes the data point at 1050 °C. At this temperature, anorthoclase is still significantly more ordered than sanidine. Therefore, the deviation from a straight line is expected to become noticeable only at temperatures higher than was the case for sanidine.

The apparent equilibrium temperature of the natural anorthoclase [$X_{Al}^{T_1} = 0.2936(14)$], as obtained from Equation 13, is T_{ae} = 798(33) °C. In contrast to sanidine, the error in T_{ae} results mainly from the error in $X_{Al}^{T_1}$, whereas the influence of the errors in slope and intercept is very small.

Table 8. Rate constants $C_o\vec{k}$, equilibrium constants K_d and Al,Si equilibrium distributions $X_{Al}^{T_1}(t_\infty)$ for anorthoclase

T (°C)	$X_{Al}^{T_1}(t_\infty)$	K_d	$C_o\vec{k}$ (d^{-1})
650	0.2990(20)	0.5898(130)	0.00113(57)
750	0.2957(10)	0.6115(67)	0.0756 (378)
850	0.2915(5)	0.6403(35)	0.305 (153)
1050	0.2850(10)	0.6871(74)	

Note: Errors given in parentheses refer to the last digits. The errors in $X_{Al}^{T_1}$ were estimated from the fit of data in Figure 6, those of K_d were calculated from the error propagation law applied to Equation 4. The error in $C_o\vec{k}$ was assumed to be ±20%.

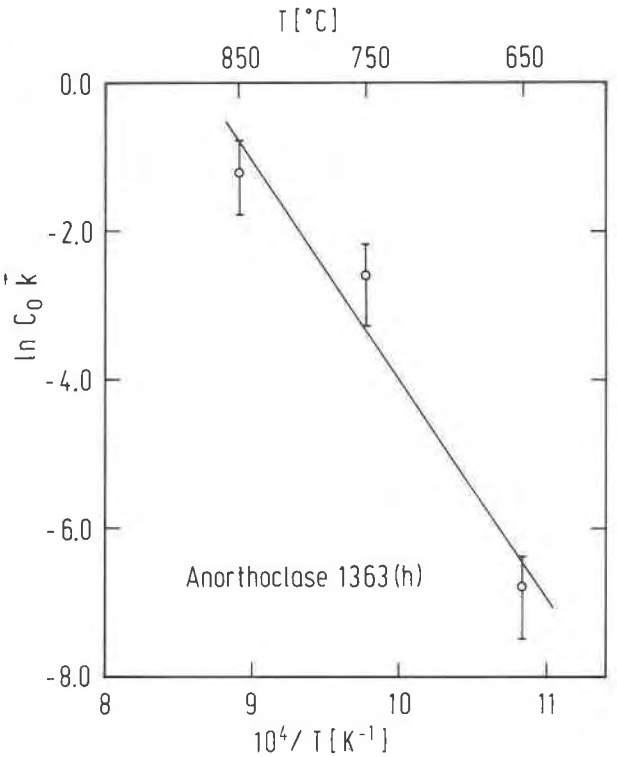

Fig. 7. Arrhenius diagram for rate constants $C_o\vec{k}$ in anorthoclase. The values of $C_o\vec{k}$ were taken from Figure 6.

Comparison of sanidine and anorthoclase

Figures 3 and 6 show that sanidine and anorthoclase have similar ordering kinetics. The rate constants and their temperature dependence, i.e., the activation energies, are similar. Sanidine and anorthoclase order at comparable rates. This finding is in contrast to a common, widespread misunderstanding in the literature, namely

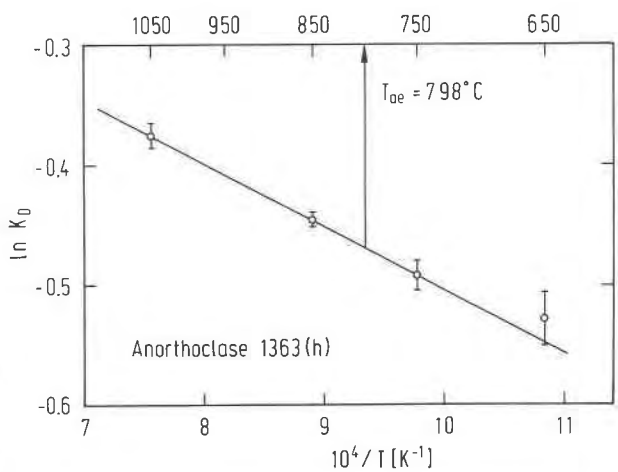

Fig. 8. Equilibrium distribution coefficients K_d of anorthoclase vs. temperature. The values K_d were calculated from $X_{Al}^{T_1}$ (t_∞) given in Figure 6.

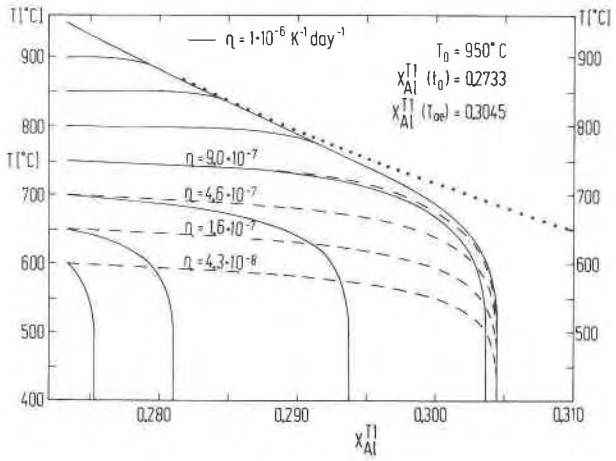

Fig. 9. Increase in order during cooling of sanidine. The degree of order $X_{Al}^{T1} = 0.3045$ of the natural material is reached if cooling begins at $T \geq 800$ °C at a rate given by $\eta = 1 \cdot 10^{-6}$/K/d (solid curves). If the crystal is quenched to $T < 800$ °C, the cooling rate constant must be decreased as indicated to allow the crystal to reach $X_{Al}^{T1} = 0.3045$ (dashed curves). The dotted curve is the equilibrium curve.

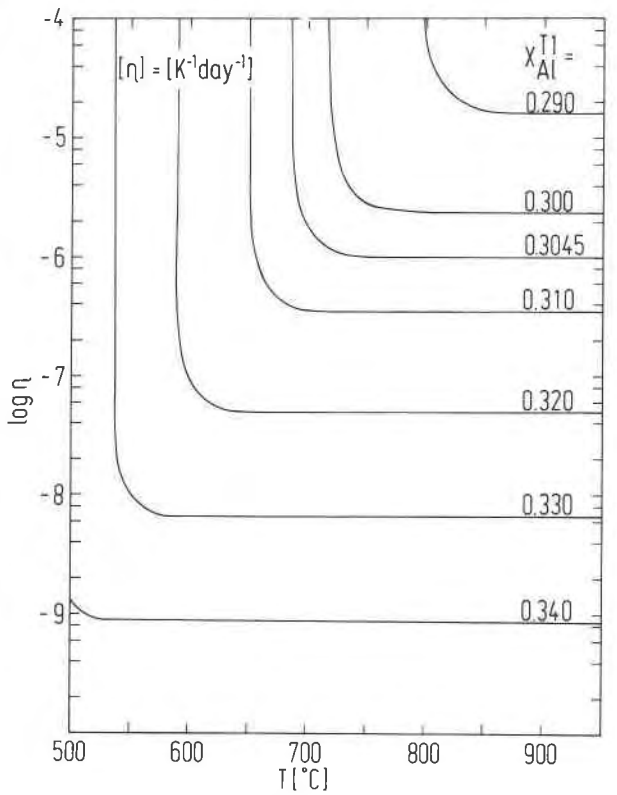

Fig. 10. Summary of cooling rate calculations for sanidine, assuming cooling from equilibrium states. The curves indicate the degree of order that will be reached if the sample is cooled from an equilibrium temperature T at a rate given by η.

that Na-rich feldspars order much faster than do K-rich feldspars. This misunderstanding is probably caused by the frequent occurrence of orthoclase. Orthoclase, however, has a short range order that is similar to microcline and is often found to be metrically triclinic on a fine scale (Bambauer et al., 1989). It is macroscopically monoclinic merely as a result of coherency strain between differently oriented triclinic domains. It is this monoclinic appearance that is mistaken as evidence for slow ordering kinetics.

Although their ordering kinetics are similar, sanidine and anorthoclase are different with respect to the temperature dependence of their equilibrium Al,Si distribution. This is seen from the slope of the straight lines in the ln K_d diagrams (Figs. 5, 8). The increase in the degree of order with decreasing temperature is more pronounced with sanidine than with anorthoclase. The same result was found by E. Senderov, Moscow (written communication).

Model calculations of cooling paths

With the kinetic data at hand, we can follow the change in Al site occupancies during continuous cooling or heating processes. For a model calculation let us assume that an equilibrated sanidine was cooled from 950 °C. Let the temperature decrease according to

$$\frac{1}{T} = \frac{1}{T_0} + \eta \cdot \Delta t \qquad (14)$$

where T_0 is the starting temperature, Δt the time elapsed, and η a cooling rate constant (Ganguly, 1982). As suggested by Ganguly, the continuous cooling process is simulated by small discontinuous steps of quenching and isothermal annealing. We have chosen steps of 10 °C, but smaller steps give the same results. The increase in X_{Al}^{T1} during each step of isothermal annealing is calculated from Equation 7. With η chosen as $1 \cdot 10^{-6}$/K/d, the upper solid curve in Figure 9 is obtained. This curve closely follows the equilibrium curve (dotted line) down to ≈800 °C, because ordering is faster than cooling. Below ≈800 °C, when cooling becomes faster than ordering, the Al,Si distribution deviates more and more from equilibrium states. This causes the ordering curve to leave the equilibrium curve with increasing slope until it is nearly vertical at some poorly defined kinetic-cutoff temperature T_∞ (≈500 °C). T_∞ may be arbitrarily defined as the temperature below which a further increase in order is beyond the limits of resolution.

The cooling rate constant, η, was systematically varied in the calculations until the site occupancy $X_{Al}^{T1} = 0.3045$ found in the natural crystal was reproduced. A value of $1 \cdot 10^{-6}$/K/d corresponds to a linear cooling rate of 1.5 °C/d at 950 °C, and 0.6 °C/d at 500 °C.

If the crystal is not cooled continuously from 950 °C, but is quenched first to $T_q > 800$ °C and then continuously cooled, ordering is very fast near T_q as a result of the deviation from equilibrium at a relatively high tem-

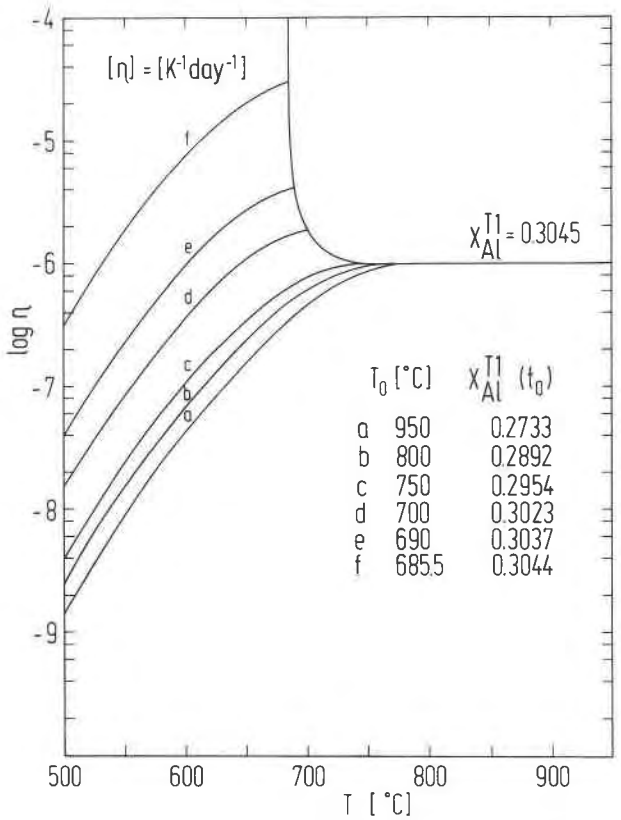

Fig. 11. Summary of cooling rate calculations for sanidine, assuming cooling from nonequilibrium states. If the sample is quenched from an equilibrium temperature T_0(a . . . f) to a lower temperature and is then continuously cooled, the rate constant η necessary to allow the crystal to reach X_{Al}^{T1} = 0.3045 can be read from the appropriate curve a . . . f.

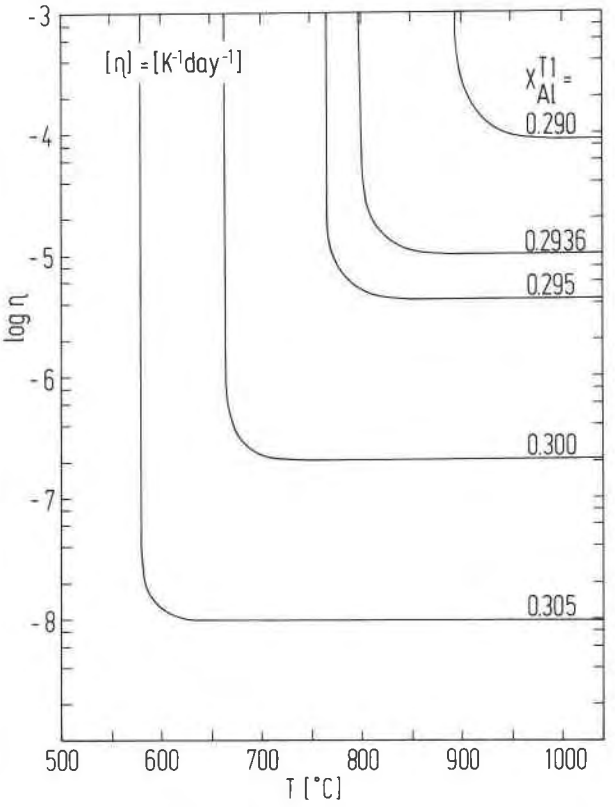

Fig. 12. Summary of cooling rate calculations for anorthoclase, assuming cooling from equilibrium states. The curves indicate the degree of order that will be reached if the sample is cooled from an equilibrium temperature T at a rate given by η.

perature, so that the equilibrium curve is reached within a few degrees of cooling, and the same final value of X_{Al}^{T1} is attained as before. However, if the crystal is quenched to T_q < 800 °C, ordering is frozen at X_{Al}^{T1} < 0.3045, so that lower cooling rates have to be applied if X_{Al}^{T1} = 0.3045 is to be reached.

The results of cooling rate calculations are summarized for sanidine in Figures 10 and 11, and for anorthoclase in Figures 12 and 13. In calculating these figures, it was assumed (1) that during cooling $P(H_2O)$ was constant at 1 kbar, and (2) that the Al,Si distribution was equilibrated at the temperature at which cooling began. Figures 10 and 12 are read in the following way. Let cooling begin at a given temperature and proceed at such a rate that a certain degree of order X_{Al}^{T1} is finally reached. Using the appropriate X_{Al}^{T1} curve, the cooling rate parameter η that allows the crystal to attain this degree of order can be found on the ordinate. For example, assume that a sanidine crystal is cooled from T_0 > 730 °C and finally reaches X_{Al}^{T1} = 0.3045. From the curve labeled 0.3045, η is found to be $\approx 1 \cdot 10^{-6}$/K/d. Above 730 °C the curve is nearly horizontal. The slight deviation from a horizontal slope between 800 °C and 730 °C may be ignored. However, if T_0 is lower than ≈730 °C, η rapidly increases because the crystal must be cooled faster when the starting temperature approaches 685 °C, the equilibrium temperature for X_{Al}^{T1} = 0.3045. From this limiting temperature, the crystal would have to be quenched at an infinite rate to preserve its state of order.

That the curve is practically horizontal above 730 °C can be interpreted as follows. If, at temperatures above ≈730 °C, cooling proceeded slower than given by $\eta = 1 \cdot 10^{-6}$/K/d, the final value X_{Al}^{T1} would not be larger than 0.3045, provided η was equal to $1 \cdot 10^{-6}$/K/d at ≈730 °C and remained so at lower temperatures. Furthermore, above ≈730 °C, cooling could also have been faster than given by $\eta = 1 \cdot 10^{-6}$/K/d without causing X_{Al}^{T1} to become less than 0.3045, again provided that η was equal to $1 \cdot 10^{-6}$/K/d at ≈730 °C. This is seen from Figure 11, where quenching is considered as the limiting case for fast cooling. If a sanidine crystal is quenched from an equilibrium temperature T_0 = a . . . e to a lower temperature and is then continuously cooled to reach X_{Al}^{T1} = 0.3045, the cooling rate constant η is found from the respective curve. For example, if the crystal is quenched from T_0 = 800 °C to 550 °C, it must be cooled according to $\eta \approx 1 \cdot 10^{-8}$/K/d

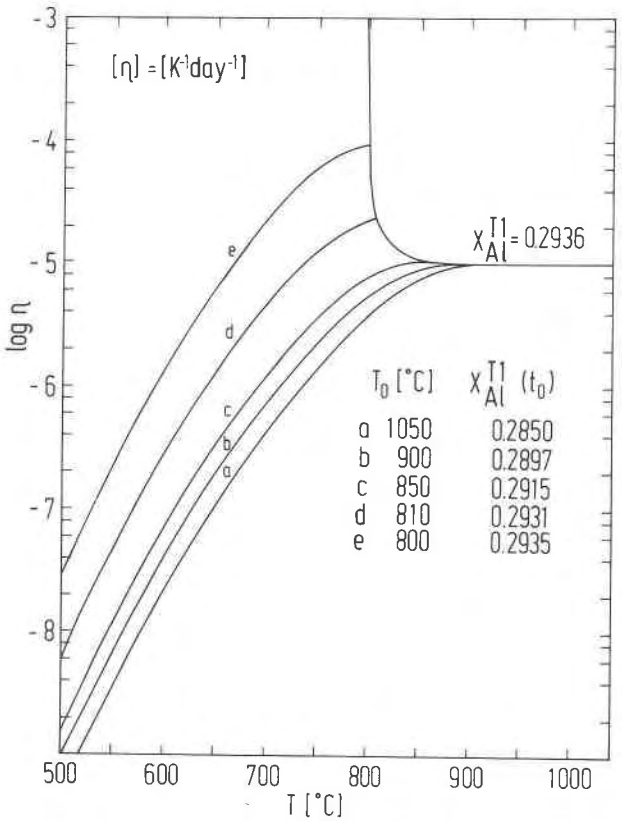

Fig. 13. Summary of cooling rate calculations for anorthoclase, assuming cooling from nonequilibrium states. If the sample is quenched from an equilibrium temperature T_0(a . . . e) to a lower temperature and is then continuously cooled, the rate constant η necessary to allow the crystal to reach $X_{Al}^{T1} = 0.2936$ can be read from the appropriate curve a . . . e.

to reach $X_{Al}^{T1} = 0.3045$ (curve b). However, if it is quenched to $T > 730$ °C, $\eta \approx 1 \cdot 10^{-6}$/K/d would still apply.

It is clear from this discussion that, for a sanidine crystal with $X_{Al}^{T1} = 0.3045$, the cooling history above ≈730 °C cannot be recovered. All that we can say is that if cooling started at $T > 730$ °C, η must have been equal to $1 \cdot 10^{-6}$/K/d at ≈730 °C, provided it did not change between 730 °C and the kinetic-cutoff temperature. This may appear to be a rather restrictive result. However, there is no need to know the actual temperature from which the crystal in question has been cooled, as long as it is known or can be determined from petrographic reasoning that the starting temperature was higher than ≈730 °C. The temperature at 730 °C is only ≈50 °C above the apparent equilibrium temperature $T_{ae} = 685$ °C, which is the lowest temperature from which cooling could have started at all.

A discussion of anorthoclase provides results analogous to sanidine (Figs. 12, 13). We can thus summarize for alkali feldspars in general. (1) If continuous cooling began at $T_0 > (T_{ae} + 50$ °C), the cooling rate at $T \approx (T_{ae} + 50$ °C) can be recovered from the ordering state, regardless of the temperature at which cooling began and the rate at which it proceeded for $T > (T_{ae} + 50$ °C). (2) If continuous cooling started at T_0 in the interval between T_{ae} and $T_{ae} + 50$ °C, we must know T_0 to find the cooling rate. (3) If continuous cooling began after the crystal had been quenched from T_0 to T_q, we must know both T_0 and T_q to determine the cooling rate. Statements 1–3 implicitly assume that the cooling rate parameter η is constant between ($T_{ae} + 50$ °C) and T_∞.

What can be said about the cooling history of the Volkesfeld and Gran Canaria crystals? We know that the Volkesfeld sanidine was quenched. Therefore, the temperature of the crystals prior to the eruption of the lava must have been close to 685 °C. The Gran Canaria anorthoclase occurs in an ignimbrite. The crystals were cooled under a H_2O pressure of less than 1 kbar. Our calculations do not apply to this situation. Further investigation of the Al,Si exchange kinetics at various pressures of $P(H_2O)$ shows that the activation energy rapidly increases with decreasing $P(H_2O)$ (Papageorgiou, personal communication; see also Yund and Tullis, 1980, for sodium feldspar). Therefore, the crystals could not have ordered much further after they were embedded in the ignimbrite. It is thus the magmatic temperature which has been preserved.

In the present case, the ordering state of the sanidine and anorthoclase crystals serves as a geothermometer, not as a geospeedometer. Application of the ordering state in terms of a speedometer and as an indicator for $P(H_2O)$, however, was successful in the case of potassium feldspars from the Ballachulish contact aureole, northwest Scotland (Kroll et al., 1991).

Continuous vs. discontinuous cooling

When a crystal is quenched from an equilibrium temperature to a lower temperature and is then isothermally annealed, ordering states result that are different from those acquired during continuous cooling. A comparison is made in Figures 14 and 15. In Figure 14, continuous cooling starts at 800 °C at the equilibrium value $X_{Al}^{T1} = 0.2892$. Three different cooling rates are applied, resulting in three different final ordering states and kinetic-cutoff temperatures, T_∞ (Table 9), ignoring for the time being the transformation of sanidine to orthoclase or microcline at ≈480 °C.

If, however, the sample is quenched from 800 °C to a lower temperature T_q and then held at this temperature as long as continuous cooling would have taken from 800 °C to T_q, the ordering states shown in Figure 15 are reached. This diagram is formally equivalent to a TTT diagram. In contrast to continuous cooling, where X_{Al}^{T1} steadily increases with decreasing temperature, a maximum state of order is reached during discontinuous cooling at a characteristic temperature, which in a TTT diagram is interpreted as the kinetic-cutoff temperature. The driving force for ordering, which is provided by the difference between the equilibrium value X_{Al}^{T1} and the constant starting value $X_{Al}^{T1} = 0.2892$, increases with decreas-

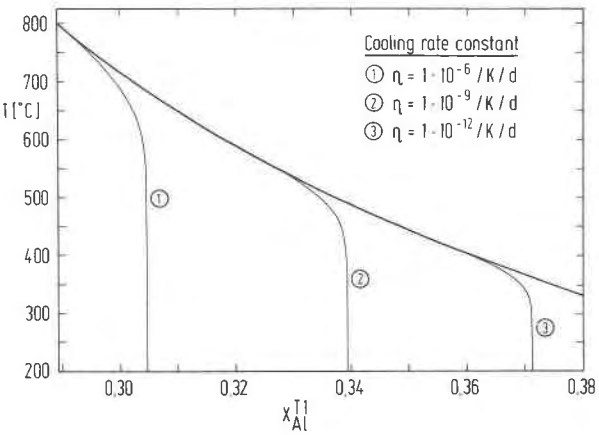

Fig. 14. States of order acquired by sanidine at different cooling rates. The sanidine-microcline transition is ignored. When sanidine is cooled at a rate greater than that given by $\eta = 1 \cdot 10^{-9}$/K/d, ordering is frozen at the sanidine structural state.

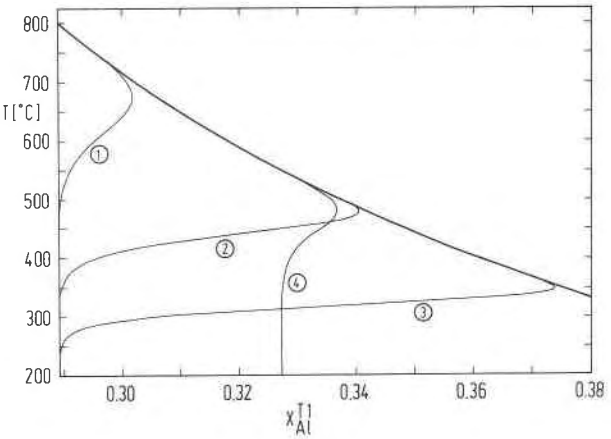

Fig. 15. States of order acquired by sanidine when it is quenched from T_0 to lower temperatures T_q and is then held at T_q for the same time as continuous cooling would have taken from T_0 to T_q, applying the same cooling rate constants η as in Figure 14. Curve 1: T_0 = 800 °C, $\eta = 1 \cdot 10^{-6}$/K/d. Curve 2: T_0 = 800 °C, $\eta = 1 \cdot 10^{-9}$/K/d. Curve 3: T_0 = 800 °C, $\eta = 1 \cdot 10^{-12}$/K/d. Curve 4: T_0 = 550 °C, $\eta = 1 \cdot 10^{-9}$/K/d.

ing temperature. At the same time, kinetics slow, so that a maximum state of order must result at some intermediate temperature.

The ordering curves for discontinuous cooling follow the equilibrium curve to lower temperatures than do the curves for continuous cooling. The difference in the temperatures at which the curves diverge increases with decreasing cooling rate, so that at low rates a state of maximum order is achieved that is larger for discontinuous than for continuous cooling. The stronger adherence to the equilibrium curve of the isothermal ordering curve results from the difference between the equilibrium and the starting values of X_{Al}^{T1}, which at all temperatures is larger for discontinuous than for continuous cooling.

The influence of this driving force becomes apparent when comparing curves 2 and 4 in Figure 15. To construct curve 4, it is assumed that the crystal is quenched from an equilibrium temperature of 550 °C, where curve 2 in Figure 10 departs from the equilibrium curve, and is then held at some lower temperature for the same time as continuous cooling would have taken from 550 °C to this temperature. Although the total time of heat treatment below 800 °C is the same for crystals 2 and 4, crystal 4 reaches a state of maximum order less than that of crystal 2. The reason is that, because of the smaller difference between the equilibrium values X_{Al}^{T1} and the constant starting value of 0.3272, the driving force for ordering below 550 °C is smaller for crystal 4.

Cooling rate and the sanidine-microcline transition

The temperature of the sanidine-microcline transition is assumed to be 480 ± 20 °C (Kroll et al., 1991). At this temperature, the Al equilibrium content of the T_1 site is X_{Al}^{T1} = 0.3417. From our model calculations (Fig. 14), assuming $P(H_2O)$ = 1 kbar, it is seen that a sanidine cooled at a rate faster than that corresponding to $\eta \approx 1 \cdot 10^{-9}$/K/d would freeze in the sanidine state. At a lower cooling rate, however, it would have the kinetic potential to order further, that is to transform to orthoclase or microcline.

Other conditions of $P(H_2O)$ would require different cooling rates to allow sanidine to transform. These are investigated by Kroll et al. (1991), and the results are applied to the cooling of sanidine in the Ballachulish contact aureole, northwest Scottish Highlands.

Sources of error

Several sources of error affect the estimation of cooling rates. Pertinent questions include the following. (1) How large is the influence of an error in X_{Al}^{T1} on the estimation of η? (2) Can the results on kinetic behavior and equilibrium states be applied to other alkali feldspar compositions? (3) To what extent do the temperature dependences of ln K_d and ln $C_0\vec{k}$ deviate from a linear relation? (4) What is the influence of a varying $P(H_2O)$? (5) Is the assumption of an ideal ordering behavior (Eq. 2) justified?

Table 9. Comparison of ordering states X_{Al}^{T1} and kinetic cutoff temperatures T_∞ for various cooling rates

		Continuous cooling		Discontinuous cooling	
η (K^{-1} d^{-1})*	rate (°C/y)**	X_{Al}^{T1}	T_∞ (°C)	X_{Al}^{T1}	T_∞ (°C)
$1 \cdot 10^{-6}$	$0.28 \cdot 10^{3}$	0.3045	≈500	0.3018	676
$1 \cdot 10^{-9}$	0.28	0.3394	≈400	0.3404	479
$1 \cdot 10^{-12}$	$0.28 \cdot 10^{-3}$	0.3713	≈300	0.3740	349

* The term η = cooling rate constant in the equation $1/T = 1/T_0 + \eta \cdot \Delta t$.

** Linear cooling rate calculated at T = 600 °C.

At present these questions can be answered as follows.

1. Our measurements of $2V_X$ are internally consistent and the error in $X_{Al}^{T_1}$ is small: ± 0.001 to ± 0.002 (Tables 5 and 7). The resultant error in η can be found from Figures 10 and 12 and is negligible. However, if $X_{Al}^{T_1}$ is determined from lattice parameters, the error may be as large as ± 0.01. This causes an error in η that is close to one order of magnitude.

2. The temperature dependences of the rate constants of sanidine and anorthoclase are the same within error (Eqs. 10 and 12). For the time being, it may be assumed that this is true for all topochemically monoclinic alkali feldspars. On the other hand, their equilibrium constants vary differently with temperature (Eqs. 11 and 13). Therefore, if the cooling rate of an alkali feldspar whose composition differs from our sanidine and anorthoclase is to be estimated, the variation of K_d with temperature must be redetermined.

It is not very critical which of the equations found in the literature is used for this purpose. While the absolute values of $X_{Al}^{T_1}$ will vary with the equation used, it is their temperature dependence, i.e., the slope of $\ln K_d$ with $1/T$, that is important. This may be demonstrated from the equation by Su et al. (1984):

$$2X_{Al}^{T_1} = 0.665 - 0.711 \cdot \sin^2 V_X. \qquad (15)$$

For the natural sanidine VS1 with $2V_X = 14.30°$ (Table 5), we find from Equation 15 that $X_{Al}^{T_1} = 0.3270$, whereas our Equation 9a gives 0.3050. Using $X_{Al}^{T_1} = 0.3270$ with Figure 10, η is seen to be $1 \cdot 10^{-8}$/K/d, which differs from our value of $1 \cdot 10^{-6}$/K/d by two orders of magnitude. However, if Su's equation is used throughout, we arrive at the same Arrhenius plot as before, with a nearly parallel shift of the straight line in the $\ln K_d$ plot. This means that the shape and spacing of the curves in Figure 10, and by analogy in Figures 11 to 13, do not change significantly. It is only their $X_{Al}^{T_1}$ labels that change. With the new labeling, however, the same value of η results as before.

For a rough estimate of η for a sanidine with $\approx$Or85 it may suffice to determine $X_{Al}^{T_1}$ from Equation 8 and to use Figure 10. This implicitly assumes that the shift of the $\ln K_d$ line is negligible. Equation 9, however, should not be used with a different composition, because the coefficients strongly depend on the Or content (compare Su et al., 1986).

3. Figure 5 shows that there is a curvilinear relation between $\ln K_d$ and $1/T$, especially at high temperatures, although the assumption of linearity within the given temperature range is not a bad approximation. A small deviation from linearity may also occur in the Arrhenius diagram (Fig. 4). However, the data are sparse, and further experiments by Papageorgiou (personal communication) are under way to determine the extent of the deviation.

4. Various sanidine crystals in the same hand specimen may show various degrees of order. One reason may be that various types and concentrations of defects are present that affect ordering kinetics. It suffices to mention the drastic effect that a small amount of Li has on the ordering rate (Bernotat-Wulf, 1991). Another factor may be the possible variation of the activity of H_2O during cooling of a magmatic body, which changes ordering kinetics. We have mentioned that $P(H_2O)$ affects the activation energy. E_A increases from 222 kJ/mol at 1 kbar to $\approx$375 kJ/mol under dry conditions. Therefore, it is not sufficient to look at one isolated sanidine crystal. It is necessary to get an idea of the variation of the state of order of sanidine crystals in the rock under investigation and to characterize the rock itself.

5. The assumption of an ideal ordering behavior is an approximation. However, cooling experiments show that calculated and observed ordering states match quite well (Papageorgiou, personal communication).

In conclusion, when used properly and with care, the Al,Si distribution in alkali feldspars, especially in K-rich alkali feldspars, is a potential geothermometer and geospeedometer. This paper has presented some initial results, and more calibrations are necessary. In particular, sanidine that has experienced different cooling rates in a lava pile should be investigated.

Acknowledgments

We would like to thank H.U. Schmincke, Kiel, for generously providing the anorthoclase crystals. W. Maresch, Münster, improved the English text. G.L. Hovis, Easton, Pennsylvania, I. Parsons, Edinburgh, and R.A. Yund, Providence, Rhode Island, made helpful comments. I. Schmiemann carefully determined sanidine and anorthoclase lattice parameters and drew the figures. G. von Cölln typed the manuscript, C. Middendorf did the photographic work. We owe our thanks to all of them.

This work was supported by the Deutsche Forschungsgemeinschaft within a program on the kinetics of rock- and mineral-forming processes, which is gratefully acknowledged.

References cited

Anovitz, L.M., Essene, E.J., and Dunham, W.R. (1988) Order-disorder experiments on orthopyroxenes: Implications for the orthopyroxene geospeedometer. American Mineralogist, 73, 1060–1073.

Bambauer, H.U., Krause, C., and Kroll, H. (1989) TEM-investigation of the sanidine/microcline transition across metamorphic zones: The K-feldspar varieties. European Journal of Mineralogy, 1, 47–58.

Bernotat-Wulf, H. (1991) Das Temperverhalten des Sanidins von Volkesfeld (Eifel). IV. Der Einfluß von Lithium auf den Ordnungs-/Unordnungsvorgang in Sanidin von Volkesfeld (Eifel) und "Orthoklas" von Madagaskar. European Journal of Mineralogy, in press.

Bertelmann, D., Förtsch, E., and Wondratschek, H. (1985) On the annealing behaviour of sanidines: The exceptional case of Eifel sanidine megacrystals. Neues Jahrbuch für Mineralogie Abhandlungen, 152, 123–141.

Besancon, J.R. (1981) Rate of cation ordering in orthopyroxenes. American Mineralogist, 66, 965–973.

Blasi, A., Brajkovic, A., and De Pol Blasi, C. (1984) Dry heating of low microcline to high sanidine via a one-step disordering process. Bulletin de Minéralogie, 107, 423–435.

Eberhard, E. (1967) Zur Synthese der Plagioklase. Schweizerische Mineralogische und Petrographische Mitteilungen, 47, 385–398.

Ganguly, J. (1982) Mg-Fe order-disorder in ferromagnesian silicates: II. Thermodynamics, kinetics, and geological applications. In S.K. Saxena, Ed., Advances in physical geochemistry, p. 58–99. Springer, New York.

Ganguly, J., and Saxena, S.K. (1987) Mixtures and mineral rocks. 291 p. Springer-Verlag, New York.

Goldsmith, J.R. (1988) Enhanced Al/Si diffusion in $KAlSi_3O_8$ at high pressures: The effect of hydrogen. Journal of Geology, 96, 109–123.

Goldsmith, J.R., and Jenkins, D.M. (1985) The high-low albite relations revealed by reversal of degree of order at high pressures. American Mineralogist, 70, 911–923.

Güttler, B., Salje, E., and Ormerod (1989) Infrared spectroscopy and the kinetics of Al,Si-ordering in Na-feldspar. Zeitschrift für Kristallographie, 128, 110–111.

Hovis, G.L. (1988) Enthalpies and volumes related to Na-K mixing and Al-Si order/disorder in alkali feldspars. Journal of Petrology, 29, 731–733.

Knitter, R. (1985) Kinetik des Al,Si-Ordnungs/Unordnungs-prozesses in Alkali-Feldspäten. Diplomarbeit, Westfälische Wilhelms-Universität Münster.

Kroll, H., and Ribbe, P.H. (1983) Lattice parameters, composition and Al,Si order in alkali feldspars. In Mineralogical Society of America Reviews in Mineralogy, 2, 57–99.

——— (1987) Determining (Al,Si) distribution and strain in alkali feldspars using lattice parameters and diffraction-peak positions: A review. American Mineralogist, 72, 491–506.

Kroll, H., Bambauer, H.-U., and Schirmer, U. (1980) The high albite-monalbite and analbite-monalbite transitions. American Mineralogist, 65, 1192–1211.

Kroll, H., Krause, C., and Voll, G. (1991) Disordering, re-ordering and unmixing in alkali-feldspars from contact-metamorphosed quartzites of the Ballachulish aureole, NW-Scotland. In G. Voll, J. Töpel, and F. Seifert, Eds., Equilibrium and kinetics in contact-metamorphism: The Ballachulish igneous complex and its aureole. Springer-Verlag, Heidelberg.

MacKenzie, W.S. (1957) The crystalline modifications of $NaAlSi_3O_8$. American Journal of Science, 255, 481–516.

Martin, R.F. (1969) The hydrothermal synthesis of low albite. Contributions to Mineralogy and Petrology, 23, 323–339.

Mason, R.A. (1979) The ordering behaviour of albite in aqueous solution at 1 kbar. Contributions of Mineralogy and Petrology, 68, 269–273.

——— (1980) Changes in the crystal morphology of synthetic reedmergnerite ($NaBSi_3O_8$) during ordering experiments. Mineralogical Magazine, 43, 905–908.

McConnell, J.D.C., and McKie, D. (1960) The kinetics of the ordering process in triclinic $NaAlSi_3O_8$. Mineralogical Magazine, 32, 436–454.

McKie, D., and McConnell, J.D.C. (1963) The kinetics of the low-high transformation in albite under dry conditions. Mineralogical Magazine, 33, 581–588.

Medenbach, O. (1985) A new microrefractometer spindle-stage and its application. Fortschritte der Mineralogie, 63, 111–133.

Mueller, R.F. (1967) Model for order-disorder kinetics in certain quasi-binary crystals of continuously variable composition. Journal of Physics and Chemistry of Solids, 28, 2239–2243.

——— (1969) Kinetics and thermodynamics of intracrystalline distribution. Mineralogical Society of America, Special Paper, 2, 83–93.

Müller, G. (1970) Der Ordnungs-Unordnungs-Übergang in getemperten Mikroklinen und Albiten. Zeitschrift für Kristallographie, 132, 212–227.

O'Neill, H.St.C., and Navrotsky, A. (1983) Simple spinels: crystallographic parameters, cation radii, lattice energies, and cation distribution. American Mineralogist, 68, 181–194.

——— (1984) Cation distributions and thermodynamic properties of binary spinel solid solutions. American Mineralogist, 69, 733–753.

Salje, E.K.H., and Kroll, H. (1991) Kinetic rate laws derived from order parameter theory III: Al,Si ordering in sanidine. Physics and Chemistry of Minerals, 17, 563–568.

Saxena, S.K., Tazzoli, V., and Domeneghetti, M.C. (1987) Kinetics of Fe^{2+}-Mg distribution in aluminous orthopyroxenes. Physics and Chemistry of Minerals, 15, 140–147.

Seifert, F. (1977) Reconstruction of rock cooling path from kinetic data on the Fe^{2+}-Mg exchange reaction in anthophyllite. Philosophical Transactions of the Royal Society of London, A 286, 303–311.

Seifert, F., and Virgo, D. (1975) Kinetics of Fe^{2+}-Mg order-disorder reaction in anthophyllites: Quantitative cooling rates. Science, 188, 1107–1109.

Senderov, E.E., and Yas'kin, G.M. (1975) Conversion of sanidine to microcline under hydrothermal conditions. Geochemistry International, 12, 139–145.

——— (1976) On stability of monoclinic potash feldspars. Geochimija, 7, 138–154 (in Russian).

Skøgby, H. (1987) Kinetics of intracrystalline order-disorder reactions in tremolite. Physics and Chemistry of Minerals, 14, 521–526.

Snow, E., and Yund, R.A. (1988) Origin of cryptoperthites in the Bishop tuff and their bearing in its thermal history. Journal of Geophysical Research, 93, 8975–8984.

Su, S.C., Bloss, F.D., Ribbe, P.H., and Stewart, D.B. (1984) Optic axial angle, a precise measure of Al,Si ordering in T_1 tetrahedral sites of K-rich alkali feldspars. American Mineralogist, 69, 440–448.

Su, S.C., Ribbe, P.H., and Bloss, F.D. (1986) Alkali feldspars: Structural state determined from composition and optic axial angle $2V$. American Mineralogist, 71, 1285–1296.

Yund, R.A. (1986) Interdiffusion of NaSi-CaAl in peristerite. Physics and Chemistry of Minerals, 13, 11–16.

Yund, R.A., and Tullis, J. (1980) The effect of water, pressure, and strain on Al/Si order-disorder kinetics in feldspar. Contributions to Mineralogy and Petrology, 72, 297–302.

Zeipert, C., and Wondratschek, H. (1981) Ein ungewöhnliches Temperverhalten bei Sanidinen von Volkesfeld/Eifel. Neues Jahrbuch für Mineralogie Monatshefte, 9, 407–415.

Manuscript received December 20, 1989
Manuscript accepted February 8, 1991